Multi-Scale Study on the Secondary Reactions of Fluid Catalytic Cracking Gasoline

Bo-lun Yang, Xiao-Wei Zhou, Xiao-Hui Yang, Chun Chen, and Long-Yan Wang
Dept. of Chemical Engineering, State Key Laboratory of Multiphase Flow in Power Engineering, Xi'an Jiaotong University, Xi'an 710049, P.R. China

DOI 10.1002/aic.11795
Published online June 16, 2009 in Wiley InterScience (www.interscience.wiley.com).

Multi-scale model considered the heat transfer, mass transfer, momentum transfer, fluid flow with reactions together at different spatiotemporal scales for the riser reactor of secondary reactions of fluid catalytic cracking gasoline (SRFCCG) process has been preformed in this work. Micro-scale of kinetics in catalyst particles, meso-scale of clusters, voids, dense phase, dilute phases, and heterogeneous structures in gas–solid flow, and the macro-scale of product distribution over riser reactor have been established using multi-scale modeling method and integrated by the multi-domain strategy. The proposed model was solved with the software of EQUATRAN-G. Good agreement between simulation results and the experimental data suggested that the proposed model was well constructed and simulation exercise was successful. The multi-scale model was capable of predicting heterogeneous structures of multi-phase flow, reactor temperature profile, and product distribution of SRFCCG process. © 2009 American Institute of Chemical Engineers *AIChE J,* 55: 2138–2149, 2009
Keywords: fluid catalytic cracking gasoline, secondary reactions, olefin, eight-lump model, multi-scale

Introduction

Automotive exhaust remains one of the leading urban air pollution sources and gains more social concern. The quality indexes of gasoline produced by China are still in an unfavorable condition, such as high olefins content, high sulfur content, high aromatics content, low octane number, and dark color. As the key component of gasoline, olefins are harmful not only for the stable performance of gasoline, but also for the life-span of automobile engine, and their content is up to 40–65 vol %, far beyond the new specification of less than 18 vol % olefins in gasoline. What's more, photochemical reactions of easily volatile olefins discharged by gasoline engines have negative effects on the environment scale. Since emission standards become increasingly stringent, production of clean fuel gasoline will be thus the primary means of suppressing air pollution from mobile source emissions.

Over the past decades, significant research efforts have been devoted in fluid catalytic cracking (FCC) gasoline to produce clean fuel. As a successful way of reducing olefins in FCC units, SRFCCG have gained more attention recently, because not only they can minimum olefins and sulfur to obtain clean gasoline, but also they can increase valuable propylene and iso-butylenes significantly. Secondary reactions for gasoline were initially proposed by John and Wojciechowski[1] in 1975, and great efforts have been devoted for this field by several researchers in recent years.

Shan and coworkers[2] reported an experimental study on the secondary reactions of gasoline in a two-stage riser reactor. Wang et al.[3] carried out an experimental study to satisfy the increasing propylene yield by reprocessing FCC naphtha in an auxiliary riser reactor. You et al.[4] preformed a nine-lump kinetic model for the aromatization reaction of FCC gasoline. Raymond et al.[5] and Ye et al.[6] developed new catalysts for

Correspondence concerning this article should be addressed to B.-l. Yang at blunyang@mail.xjtu.edu.cn

© 2009 American Institute of Chemical Engineers

reducing FCC gasoline olefins, which selectively promoted certain secondary reactions like olefins cracking and hydrogen transfer by introducing special active substance into catalysts. The authors[7] proposed a new process for reducing gasoline olefin and increasing propylene yield, which provided with independent reaction time, reaction space, and favorable conditions for FCC gasoline secondary reactions in a separate riser reactor. Experimental study and molecular simulation using method of Structure Oriented Lumping combined with Monte Carlo for secondary reactions of FCC gasoline have also been reported in our pervious works.[8,9] An Eight-lump kinetic model[10] for SRFCCG has been proposed based on the assumption of ideal plug flow.

It can be noted that past efforts made in the field of secondary reactions of FCC gasoline have been limited to the new technology development, experimental study, and the kinetics. These researches did not take into account the detailed information of mass transfer, momentum transfer, heat transfer, especially for its heterogeneous structures in the riser reactor of SRFCCG.

In fact, SRFCCG in the riser reactor is characterized by thousands of reactions far away from chemical equilibrium, high non-linearity and heterogeneity, close coupling and multiplicity, bifurcation and dynamic behavior. However, detail mathematic description for the riser reactor of SRFCCG, which considers all these aspects comprehensively, has not been reported yet. Hence, it is significant and necessary to develop a new way to model SRFCCG systematically and to meet the worldwide need for FCC units of producing clean fuel gasoline with low olefins.

For modeling multi-phase reactor, several methods have been reported in available literatures, such as flow-reaction model using Eulerian multi-fluid approach by Gao et al.[11] and three-dimensional mathematical model using computational fluid dynamics techniques by Theologos et al.[12] However, reactor model established by these methods focused on the product distribution prediction at the macro-scale of reactor size, without accounting for detailed information at different spatiotemporal scales and their complex relationship. On the other hand, as a new method to describe the transfer phenomena, multi-scale relation and coupling of multi-phase flow in fluidization bed, the energy-minimization multi-scale (EMMS) model proposed by Li et al.[13–15] has obtained many attentions recently. However, complex reaction system has not been taken into account in their model.

From the above consideration, a new model which included multi-phase flow, mass transfer, heat transfer, and momentum transfer with heterogeneous catalytic reactions together for the riser reactor of SRFCCG is proposed in this work. The objective of this work is to reveal the multi-scale characteristics of non-linearity, non-equilibrium, unsteady state, and heterogeneous structure and to predict parameters of interest at different spatiotemporal scales in the riser reactor of SRFCCG. It is different from the traditional modeling methods for multi-phase reactor, a multi-scale approach is first adopted to construct a multi-scale model for the riser reactor of SRFCCG in this work. Also, it is different from the strategy of EMMS model, three subscale models, which are micro-scale of catalytic kinetics in catalyst particles, meso-scale of clusters, voids, dense phase, dilute phases, and heterogeneous structures in gas–solid flow and macro-scale of reactor product distributions, have been established and integrated by multi-domain strategy[16] in the proposed multi-scale model. This new model is solved with the software of EQUATRAN-G developed by Omega Simulation, (OSC), Japan, and the simulation results are compared with experimental data.

Multi-Scale Modeling Approach

Chemical engineering multi-scale approach first proposed by Davis in 1901, has been widely used currently. Micro-reactions in chemical engineering process are dominated by interaction of diffident scales. Only in this way can it reach ideal conversion and selectivity at the scale of reactor size, then output qualified and low-cost products at the scale of factory size, simultaneously minimize the negative effects on the scale of environment size.

The system of SRFCCG is characterized by typically heterogeneous gas–solid two-phase flow and dissipative structure with non-linear, non-equilibrium, unsteady state, and multi-scale nature. In this study, the system has been decomposed into following three subsystems based on the consideration of structure and scale.

1 Micro-scale subsystem of catalytic kinetics in catalyst particles. Micro-scale interaction is correlated with the catalytic cracking reaction of hydrocarbons vapor on catalysts, which is complex parallel-series reaction in carbonium ion mechanism. Reactions involved here are cracking, isomerization, hydrogen transfer, aromatization, alkylation, condensation, and coke-formation reactions. Chemical potentials play extremely important role in the micro-scale.

2 Meso-scale subsystem of cluster, voids, dense phase, dilute phases, and heterogeneous structures in gas–solid flow. Meso-scale interaction occurs in dispersed clusters with dilute phase, dense phase, and inter-phase of the gas–solid suspension. Because of the coalescence and breakup of clusters, heterogeneous structures in gas–solid flow are formed in the meso-scale. Meso-scale boundaries are the local verges of dense phase and dilute phase.

3 Macro-scale subsystem of product distributions in riser reactor. Macro-scale interaction is related with the interaction in the overall riser reactor and the boundaries such as the internal wall borderlines, the inlet and outlet of riser reactor, and inter-verges of core-annulus zone.

In this model, the ideal and non-ideal reactions between lumps of SRFCCG have been taken into account at the micro-scale of catalytic kinetics in catalyst particles. Two-dimensional heterogeneous distributions of dynamic parameters, such as voidage, gas velocity, solid velocity, gas–solid slip velocity, coalescence and breakup of clusters, mass transfer coefficient, energy consumption for suspending and transporting catalyst particles, and inhomogeneous coefficient have been considered at the meso-scale. Temperature profile and product distribution along with the riser height have been studied at the macro-scale. Assumptions required in this model are that once stable state of the macro-scale system is reached, dense phase and dilute phase keep exchanging, clusters coalescing and breaking at a constant frequency, and their volume fractions keep constant; it is also required that the consuming or generating mass rate for each lump during the secondary reactions is equal to the mass interchanging rate at micro-scale of catalyst particles. Sub-models

of different scales are integrated into a multi-scale model by multi-domain strategy.

Micro-scale subsystem model

Ideal and non-ideal reactions, including cracking, isomerization, hydrogen transfer, aromatization, alkylation, condensation, and coke-formation reactions have been considered in the micro-scale subsystem. The eight-lump kinetic model of SRFCCG developed in our previous work is adopted selectively to describe the complex reaction system. In this eight-lump model, DG, LPG, LCO, COKE, and GL represent dry gas lump (C1, C2), liquefied petroleum gas lump (C3, C4), light cycle oil lump (>477 K), coke lump and gasoline lump (C5+, −477 K), respectively, while GL lump is further divided into paraffin lump (GP), olefin lump (GO), naphthene lump (GN), and aromatic lump (GA). Since vapor residence time is very short, the reactions are far away from chemical equilibrium under normal operating conditions; thus, it is reasonable to treat all the reactions as first-order ones. The effects of internal and external diffusion on reactions have been eliminated. The catalyst decay is neglected and active sites ideally distribute on the surface of catalyst. A continuity equation in the riser reactor can be obtained:

$$\left(\frac{\partial \rho\alpha_j}{\partial t}\right)_z + G_v\left(\frac{\partial \alpha_j}{\partial z}\right)_t = r_j \tag{1}$$

The disappearance rate of lump j is in direct proportion to its mole concentration $\rho\alpha_j$ and the mass density of catalyst to gas volume.

$$r_j = -K_j^{'}(\rho a_j)\left(\frac{\rho_p}{\varepsilon}\right) \tag{2}$$

Equation 3 can be derived from Eqs. 1 and 2,

$$\left(\frac{\partial \rho a_j}{\partial t}\right)_z + G_v\left(\frac{\partial a_j}{\partial z}\right)_t = -K_j^{'}(\rho a_j)\left(\frac{\rho_p}{\varepsilon}\right) \tag{3}$$

When the stable state of SRFCCG is reached, the partial derivative item in the left of Eq. 3 equals to zero. One can be obtained that,

$$G_v\left(\frac{\partial a_j}{\partial z}\right)_t = -K_j^{'}(\rho a_j)\left(\frac{\rho_p}{\varepsilon}\right) \tag{4}$$

Meso-scale subsystem model

Any location in the riser reactor can be divided into dense phase, dilute phase, and inter-phase. The mechanisms of different scales inside the gas–solid flow lead to compromise between gas flow and particle flow. Particles tend to maintain themselves as low as possible with minimum potential energy, which leads to a maximal particle volume fraction in the riser reactor. Meanwhile, the fluid motion tends to consume minimum power for transporting and suspending particles per unit bed volume. Generally, neither the particles nor the fluid can dominate the other's tendency exclusively, thus they have to compromise each other to reach a stable state of the gas–solid two-phase flow system according to Li's theory.[15] At the meso-scale, heterogeneous distribution of voidage, catalyst clusters, gas velocity, and particle velocity are induced by interaction between gas flow and particle flow, consequently leading to the inhomogeneous distribution of slip velocity, then resulting in heterogeneous distribution of mass transfer coefficients at different scales.

Axial distribution of voidage

The axial distribution of voidage in a riser reactor is most likely with an S-shaped profile consisting of a dense section at the bottom and a dilute section at the top bridged by a transition section in the middle and can be calculated by the equation proposed by Kwauk and his coworkers.[17]

$$\ln\left[\frac{\varepsilon - \varepsilon_d}{\varepsilon_l - \varepsilon}\right] = -\frac{1}{z_0}(z - z_i) \tag{5}$$

with

$$\varepsilon_d = 0.484\left[\frac{18\ Re_p + 2.7\ Re_p^{1.687}}{Ar}\right]^{0.0741} \tag{6}$$

$$\varepsilon_l = 0.95\left[\frac{18\ Re_p + 2.7\ Re_p^{1.687}}{Ar}\right]^{0.02857} \tag{7}$$

$$z_0 = 500\ \exp[-69(\varepsilon_l - \varepsilon_d)] \tag{8}$$

where z_0 is the characteristic length for axial voidage profile and the inflection point of axial profile z_i can be calculated by the volume of catalyst particles in the riser reactor.

Radial distribution of voidage

Heterogeneous radial distribution of particle dense is a basic feature of gas–solid two-phase flow. As the cross-section averaged concentration of catalyst particles keeps constant, radial particle dense profile in the riser reactor can be determined by the corresponding normalized position $\phi = r/R$ only. Radial distribution of voidage is as a function of the normalized position only. Hence, equations for radial voidage distribution proposed by Cheng et al.[18] can be used.

$$\varepsilon(r) = a1 + b1 \times \left[\frac{r}{R}\right]^n \tag{9}$$

$$\bar{\varepsilon} = \frac{2}{R^2}\int_0^R \varepsilon(r)\cdot r dr \tag{10}$$

with

$$a1 = \varepsilon_0, b1 = \varepsilon_w - a1,\ n = -2 + 2 \times b1 \times (\bar{\varepsilon} - a1)^{-1} \tag{11}$$

Introducing Eqs. 10 and 11 into Eq. 9, then expression of $\varepsilon(r)$ can be obtained as:

$$\varepsilon(r) = \varepsilon_0 + (\varepsilon_w - \varepsilon_0)\left[\frac{r}{R}\right]^{\frac{2(\varepsilon_w - \varepsilon_0)}{\bar{\varepsilon} - \varepsilon_0} - 2} \tag{12}$$

where ε_0 and ε_w can be determined by the corresponding $\bar{\varepsilon}$.

$$\begin{cases} \varepsilon_0 = \varepsilon_{mf} + \dfrac{0.895 - \varepsilon_{mf}}{0.75 - \varepsilon_{mf}}(\bar{\varepsilon} - \varepsilon_{mf}) & (\bar{\varepsilon} \le 0.75) \\ \varepsilon_w = \varepsilon_{mf} \end{cases} \quad (13)$$

$$\begin{cases} \varepsilon_0 = 1 - 0.42(1 - \bar{\varepsilon}) \\ \varepsilon_w = \varepsilon_{mf} + \dfrac{\bar{\varepsilon} - \varepsilon_{mf}}{0.75 - \varepsilon_{mf}}(\bar{\varepsilon} - 0.75) & (\bar{\varepsilon} < 0.75) \end{cases} \quad (14)$$

Radial distribution of superficial gas velocity

Radial distribution of superficial gas velocity U_g in a riser reactor is characterized by a core-annulus structure, which is an especially heterogeneous structure of higher gas velocity in the core region and lower in annulus region. With increasing solid flow rate, the drag force increases, leading to richer gas in core region and denser particles in annulus region. Additionally, the increase of gas velocity gives rise to the increase of radial gas velocity and the decrease of the drag force against upward gas flow for lower particle dense in the riser reactor center, which co-result in faster increase of gas velocity in core region than that in annulus region. Expression of $U_g(r)$ by Cheng et al.[18] thus can be used.

$$U_g(r) = U_{g0}\left[1 - \frac{r}{R}\right]^{-1.5+\sqrt{2.25-2(U_g-U_{g0})/U_g}} \quad (15)$$

where U_g can be calculated by U_{g0}, generally, which is 1–2 times larger than U_g.

Slip velocity

Slip velocity U_s is an important parameter for gas–solid flows that it can be used to evaluate the level of mixture and contact for gas and solid flow. It is correlated with the transfers of mass, momentum, and the residence time distribution of catalyst particles. The phenomenon that the slip velocity is larger than the terminal fall velocity of the single particle U_{pt} indicates that clusters exist in the riser reactor. Moreover, slip velocity between dense phase and dilute phase makes the most contribution to the local slip velocity, from which the correlation of local slip velocity with local voidage can be derived. Hence, the local gas–solid slip velocities can be predicted with the correlation. Additionally, the gas–solid flows are subject not only to mass and momentum conservation but also to the stability condition of minimum energy consumed for transporting and suspending with respect to unit mass of particles according to EMMS model, and following formulations can be obtained by simply reformulating the basic equations of EMMS model.[15]

$$U_{si}(r) = U_{gl}(r) - \frac{\varepsilon_l}{1 - \varepsilon_d} U_{pd} \cdot [1 - f(r)] \quad (16)$$

$$U_{gl}(r) = [U_g(r) - \frac{\varepsilon_d}{1 - \varepsilon_d} U_p(r) - f(r) U_{sd}(r)]/[1 - f(r)] \quad (17)$$

$$U_{pd}(r) = U_p(r)/f(r) \quad (18)$$

$$U_s(r) = U_g(r) - \frac{\varepsilon(r) \cdot U_p(r)}{\varepsilon(r)} \quad (19)$$

Consequently, U_{pt} can be obtained by reformulating Eqs. 16–19.

$$U_s(r) = \frac{f(r)U_{sd}(r) + U_{si}(r)}{\varepsilon(r)} \quad (20)$$

where, U_{sd} and U_{si} can be obtained from Eqs. 21 and 22:

$$0.15\left[\frac{\rho_f d_p}{\mu}\right]^{0.687}[U_{sd}(r)]^{1.687} + U_{sd}(r) - [1 - \varepsilon(r)]\frac{\varepsilon_d^{4.7}}{1 - \varepsilon_d}\frac{(\rho_p - \rho_f)g d_p}{18\mu} = 0 \quad (21)$$

$$0.15\left[\frac{\rho_f d_d(r)}{\mu}\right]^{0.687}[U_{si}(r)]^{1.687} + U_{si}(r) - [1 - f(r)]^{5.7}(\varepsilon_l - \varepsilon_d)\frac{(\rho_p - \rho_f)g[d_d(r)]^2}{18\mu} = 0 \quad (22)$$

Radial velocity distribution of catalyst particles

There simultaneously exist both upward and downward particle flow, and core-annulus structure in riser reactor which is consisted of core region with higher particle velocity and annulus region with lower particle velocity near the wall. What's more, $U_s(r)$ is a function of $l(r)$ and $f(r)$, and can be determined by the corresponding $\varepsilon(r)$.

$$f(r) = \frac{\varepsilon_l - \varepsilon(r)}{\varepsilon_l - \varepsilon_d} \quad (23)$$

$$\frac{l(r)}{d_p} = D\frac{\varepsilon_l - \varepsilon(r)}{\varepsilon_l - \varepsilon_d} \quad (24)$$

Stability condition of minimum energy for suspending and transporting particles[15]:

$$N_{st}(r) = \min$$

One can obtain from theory of EMMS model:

$$\varepsilon_l = 1.0,\ \varepsilon_d = \varepsilon_{mf}$$

$U_s(r)$ can be calculated out with D and $\varepsilon(r)$, hence, expression of $U_P(r)$ can be obtained.

$$U_p(r) = \frac{1 - \varepsilon(r)}{\varepsilon(r)} g[U_g(r) - U_s(r)] \quad (25)$$

Mass transfer coefficient

Mass transfer coefficient Kg is a basic parameter for mass transfer process of gas–solid flow. By judging the mass transfer rate, the control step for mass transfer process can be asserted. Mass transfer coefficient at different scales in

SRFCCG system, can be calculated with slip velocity using the formulations proposed by Basu and Halder[19]

$$Sh_l = 2\varepsilon_l + 0.69\left[\frac{U_{sl}d_p}{v_g\varepsilon_l}\right]^{0.5} Sc^{0.3} \tag{26}$$

$$Sh_d = 2\varepsilon_d + 0.69\left[\frac{U_{sd}d_p}{v_g\varepsilon_d}\right]^{0.5} Sc^{0.3} \tag{27}$$

$$Sh_b = 2\varepsilon_b + 0.69\left[\frac{U_{sb}l}{v_g(1-f)}\right]^{0.5} Sc^{0.3} \tag{28}$$

$$Sh_m = 2\varepsilon + 0.69\left[\frac{U_{sm}d_p}{v_g\varepsilon}\right]^{0.5} Sc^{0.3} \tag{29}$$

Relation of Sherwood number with mass transfer coefficient can be expressed as:

$$Sh = Kg \cdot d_p/D_{ab} \tag{30}$$

Conversion between dilute and dense phase at the meso-scale

Conversion between dilute and dense phase at the meso-scale induced by coalescence and breakup of clusters maintains a constant frequency at stable state of the system. On the basis of the force analysis for the process of catalyst particles being accelerated from dense phase to dilute phase, Eqs. 31 and 32 can be obtained according to Newton's first law. F_h, F_y, F_f, F_z, and α_0 represent the resultant force, gravity, buoyancy, drag force, and particle acceleration, respectively. Integration of the acceleration is expressed as Eq. 33; integration time is precisely half of the reunion-cycle time of cluster coalescence and breakup.

$$F_h = F_y + F_f - F_z = ma_0 \tag{31}$$

$$a_0 = \frac{dU}{dt} \tag{32}$$

$$t = \int_{U_{pd}/(1-\varepsilon_d)}^{U_{pl}/(1-\varepsilon_l)} \frac{m}{F_h} dU_p = \frac{1}{2f} \tag{33}$$

Macro-scale subsystem

The uppermost problems need to be solved at the macro-scale are the sudden change in degrees of freedom, the multi-scale consistency, and the mechanism of multi-scale coupling. Interactions occurring in different phases at different scales co-lead to the heterogeneous and multi-scale structures of gas–solid two-phase flow, and the global stable state at macro-scale of product distributions in riser reactor, which is intrinsically formed by comprising of mechanism at different scales. Finally, stable state of system is reached at the scale of overall riser reactor size with the effects of boundary conditions and operating conditions.

Temperature profile of riser reactor

From the experimental operation, it can be known that the riser reactor is adiabatic one, the vaporization of gasoline is instantaneous, and all the heat needed for vaporizing gasoline and secondary reactions in the riser reactor are provided by the regenerated catalysts with high-temperature. On the basis of these considerations, the energy balance (Eq. 34) derived from expressions proposed by Moustafa and Froment[20] thus can be used. Reactor temperature profile along with the riser height can be obtained by solving the Eq. 34 with the following boundary conditions: at $z = 0$, $C_i = C_{i0}$; $C_c = C_{c0}$; $T = T_0$.

$$(m_g Cp_g + m_p Cp_p)\frac{dT}{dz} = \sum_i \sum_j \rho_s(-\Delta H)_{i,j} r_{i,j}(1-\varepsilon(z)) \tag{34}$$

Solution with respect to the lump concentration

Because of the heterogeneous flow structure constituting of gas and catalyst particles, dilute phase and dense phase, vapor mass rate in dilute phase can be written as:

$$G_{Vl} = \rho U_{gl} \tag{35}$$

Vapor mass rate in dense phase can be expressed as:

$$G_{Vd} = \rho U_{gd} \tag{36}$$

Following equations can be obtained from reformulating Eqs. 4, 34, and 35.

For dilute phase

$$U_{gl}\frac{da_{jl}}{dz} = -K_j' a_{jl}\left(\frac{\rho_p}{\varepsilon_l}\right) \tag{37}$$

$$-K_j' a_{jl}\frac{\rho_p}{\varepsilon_l} = K_{gl}a(1-\varepsilon_l)(1-f)(a_{jl}-a_{js}) + K_{gb}fa'b(a_{jl}-a_{js}) + K_{gm}mfba(a_{jl}-a_{js}) + kfda'(a_{jd}-a_{jl}) \tag{38}$$

For dense phase

$$U_{gd}\frac{da_{jd}}{dz} = -K_j' a_{jd}\left(\frac{\rho_p}{\varepsilon_d}\right) \tag{39}$$

$$-K_j' a_{jd}\frac{\rho_p}{\varepsilon_l} = K_{gd}a(1-\varepsilon_d)(a_{jd}-a_{js}) + kfda'(a_{jl}-a_{jd}) \tag{40}$$

With

$$k = 2\sqrt{\frac{D_{ab}\varepsilon_d}{\pi t}} \tag{41}$$

$$t = \frac{\pi D_d}{2\left[\frac{U_{gl}}{\varepsilon_l} - \frac{U_{gd}}{\varepsilon_d}\right]} \tag{42}$$

Table 1. Expressions of Secondary Reactions Kinetic Parameters

$k = f(T)$, m^3/g_{cal} s
$k_{GP,GO} = \exp(2.4664-2830/T)$
$k_{GP,DG} = \exp(4.3282-4329/T)$
$k_{GO,GP} = \exp(2.0565-1775/T)$
$k_{GO,LCO} = \exp(0.7626-1221/T)$
$k_{GO,DG} = \exp(3.2172-3169/T)$
$k_{GN,GO} = \exp(0.6411-867/T)$
$k_{GN,LCO} = \exp(6.4059-6720/T)$
$k_{GN,DG} = \exp(4.7073-5235/T)$
$k_{GA,GN} = \exp(-1.7427-1865/T)$
$k_{GA,COKE} = \exp(0.3454-1607/T)$
$k_{LCO,COKE} = \exp(1.7184-3126/T)$
$k_{GP,LPG} = \exp(1.6540-1888/T)$
$k_{GP,COKE} = \exp(4.3775-4920/T)$
$k_{GO,GN} = \exp(1.3698-1096/T)$
$k_{GO,LPG} = \exp(2.3665-1574/T)$
$k_{GO,COKE} = \exp(5.1227-4975/T)$
$k_{GN,GA} = \exp(1.8989-1894/T)$
$k_{GN,LPG} = \exp(1.4000-1795/T)$
$k_{GN,COKE} = \exp(3.8854-3801/T)$
$k_{GA,LCO} = \exp(1.8889-3786/T)$
$k_{LPG,DG} = \exp(-0.0837-1974/T)$

For j lump at the outlet

$$a_{jout} = (1-f)\cdot a_{jlout} + f \cdot a_{jdout} \tag{43}$$

Solution scheme of the multi-scale model

Data used for calculation in this work: diameter of catalyst particle is 60 μm, interfacial area of catalyst particle is 98 m^2/g, and particle density is 840 kg/m^3. Viscosity is 3.0×10^{-5} Pa s, kinematic viscosity is 1.6×10^{-5} m^2/s, minimum fluidized voidage is 0.4, maximum voidage is 0.9997, initial flow speed is 2.0 m/s, recycling catalyst mass rate is 60 kg/m^2 s, diffusion coefficient is 1.71×10^{-5} m^2/s, reaction rates of secondary reactions for catalytically cracking gasoline can be calculated by following expressions[10] shown in Table 1. Framework for multi-scale model solution is given in Figure 1.

As shown in Figure 1, the axial distribution of voidage can be obtained first by jointly solving Eqs. 5 and 12 with given conditions; radial distribution of fluid velocity can be calculated by Eq. 15; volume faction of dense phase can be obtained by solving Eq. 23; $l(r)$, $U_s(r)$, $U_p(r)$, $U_{sd}(r)$, and $U_{si}(r)$ can be obtained by jointly solving of Eqs. 20, 21, 22, 24, and 25. Hence, mass transfer coefficient can be calculated by Eqs. 26–30 and slip velocity. Finally, lump concentration at reactor outlet can be obtained by the simultaneous solution of Eqs. 34–43.

The proposed model is solved with the software of EQUATRAN-G developed by Omega Simulation, (OSC), Japan. This software has been successfully used to solve the problems in heat and mass transfer, fluid and particle dynamics, kinetics and reactors, and so on.[21,22]

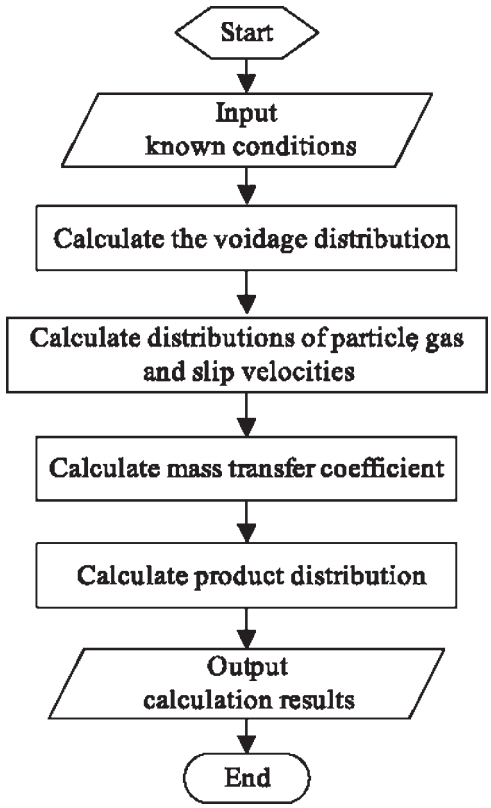

Figure 1. Flowchart of the multi-scale model solution.

Results and Discussion

Axial distribution of voidage

The axial voidage profile in riser reactor is plotted in Figure 2. It is shown that the voidage smoothly increases in low section, then sharply increases from 4.5 to 6.0 m, finally keeps almost constant at the top section with the increasing riser reactor height. Reason involved here is that recycling catalyst particles near the riser inlet, the gravitational effect of particle, and the backmixing particle co-lead to the lower denser section and the upper dilute section. The axial voidage profile provides the evidence that there exists S-shaped axial voidage profile consisting of a dense bottom and dilute-phase at the top bridged by a transition section in the middle of riser reactor, which is well fit with the characteristic of fast fluidized bed.

Radial distribution of voidage

Figure 3 shows the radial voidage distribution in riser reactor. The maximum voidage exists in the reactor center and maintains nearly unchanged in the core region, and then sharply decreases near the wall in each cross-section. Additionally, the descending rate of voidage near the wall goes up with the increasing height. It is because the core-annulus structure consisted with a high gas velocity core-dilute region and a low gas velocity annulus-dense region. What's more, with the rising height, the averaged cross-section voidage increases and the transition point is much closer to the wall. It is suggested that the upper section become more dilute and the annulus region become thinner from inlet to outlet.

Distribution of slip velocity

Slip velocity distribution is given in Figure 4. As shown in this figure, slip velocity maintains unchanged in the center, and then sharply increases near the wall at each

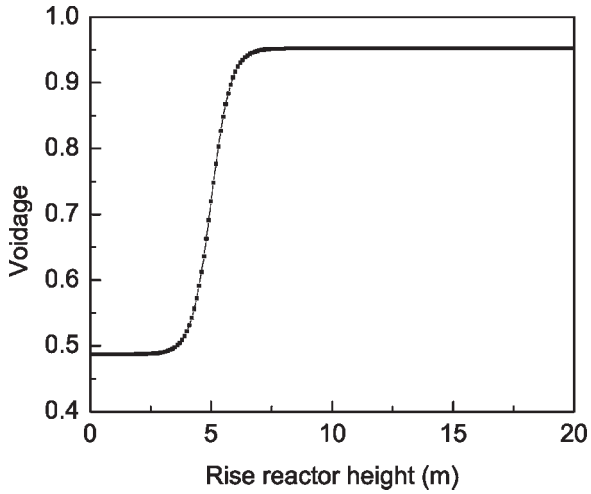

Figure 2. Axial distribution of voidage.

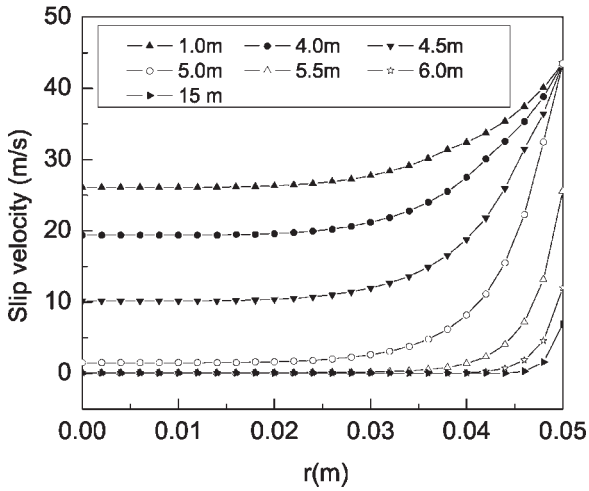

Figure 4. Distribution of slip velocity.

elevations of the riser reactor. Additionally, slip velocity increases with the rising reactor height. This is because that slip velocity is induced by the interaction between gas and particle, while relatively faint interactions in core dilute section and upper dilute section would lead to low slip velocity, relatively intense interactions in annulus dense section and lower dense section would result in high slip velocity. Hence, the intensity of the interaction between gas phase and solid phase can be authentically reflected by the local slip velocity rather than global superficial slip velocity.

Distribution of inhomogeneous coefficient

The inhomogeneous coefficient here is the ratio of equivalent cluster diameter to particle diameter, that is, $K(r) = l/d_p$. It can be used to estimate the level of radial heterogeneity and reflect the intensity level of coalescence and breakup of clusters. As shown in Figure 5, inhomogeneous coefficient keeps almost constant in the center and sharply increases towards the wall in each cross-section, the averaged inhomogeneous coefficient decreases with the increasing height. One implied the phenomenon is that annulus region is more complex and more heterogeneous than core region. The reason involved here may be that the dilute phase with fewer particles is controlled by the gas flow, which thus leads to fewer clusters and more uniform distribution in the core region and the upper section. While the denser phase is controlled by the jumbled particles, the intense contact of particles, coalescence and breakup of clusters, which leads to more inhomogeneous distribution in the annulus region and the lower section.

Distribution of energy consumption for suspending and transporting

Distribution of energy consumption for suspending and transporting with respect to unit mass of particles (N_{st}) is plotted in Figure 6. As shown in this figure, N_{st} smoothly decreases in the center and then sharply decreases near the wall in each cross-section. N_{st} is relatively small in the upper section of reactor, and much bigger in the lower section of reactor. It is because the energy consumption for suspending and transporting is proportional to the particle density at the corresponding location. Additionally, there are two transitional points, one is the height of 4.5 m, which is the critical

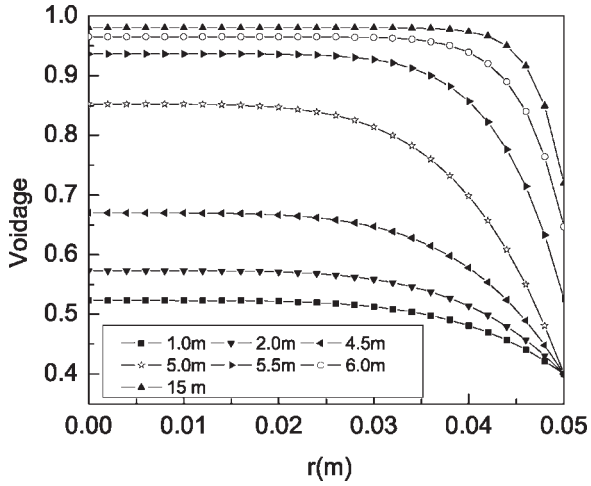

Figure 3. Radial distribution of voidage.

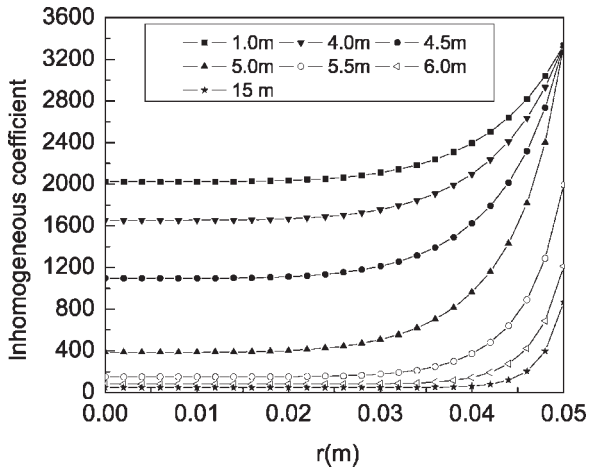

Figure 5. Distribution of inhomogeneous coefficient.

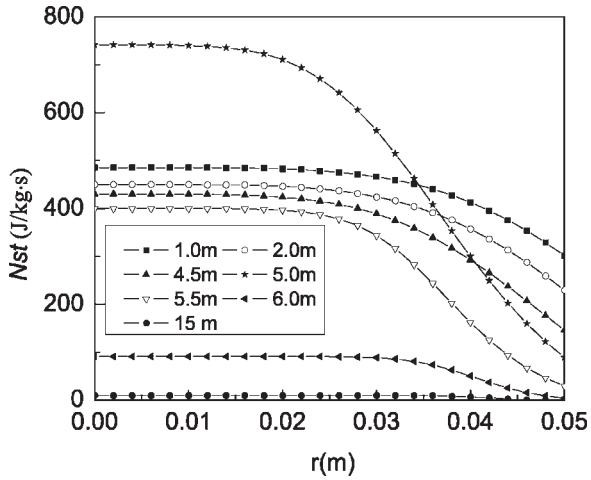

Figure 6. Distribution of energy consumption for suspending and transporting.

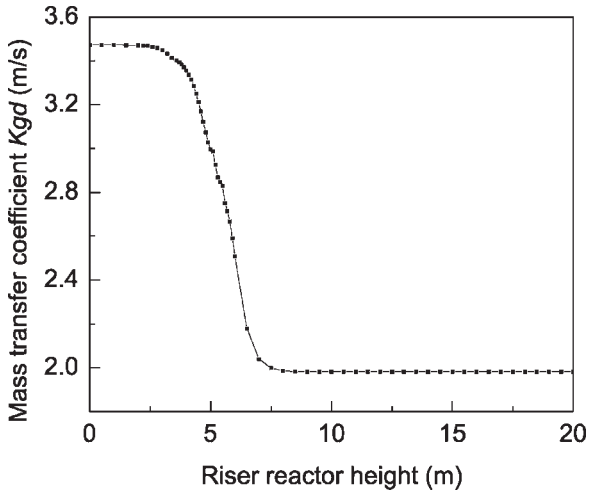

Figure 8. Axial distribution of mass transfer coefficient in dense phase.

point from dense section to transitional section, and the other is the height of 6 m, which is the critical point from the transitional section to the dilute section.

Axial distribution of mass transfer coefficient

Axial distributions of mass transfer coefficient in dilute phase and dense phase, the inter-phase between dilute phase and clusters, and the inter-phase between dilute phase and dynamic clusters are shown in Figures 7–10, respectively.

As shown in these four figures, it can be found that mass transfer coefficients at different scales have the similar changing trend, which is the mass transfer coefficient initially keeps a larger constant, and then dramatically decreases, finally maintains a smaller constant with the increasing riser reactor height. Situation here is induced by the heterogeneous and dissipative structure of the gas–solid two-phase flow in the corresponding sections. What's more, sudden change in mass transfer coefficient may be attributed to the sharp increase of slip velocity and dramatic decrease of voidage in the middle transitional section. Additionally, it can be noted that transitional section is approximately from 4.5 to 6 m. Because of the relatively high slip velocity between the fluid in dilute phase and clusters, as shown in Figure 9, mass transfer coefficient in inter-phase between dilute phase and clusters is larger than the other three mass transfer coefficients in the orders of magnitude, indicating that the overall mass transfer is dominated by the mass transfer between clusters and dilute-phase.

Verification of the model

The feedstocks, three samples of catalytically cracked gasoline used in this work, were taken from the industrial FCC units of China. Their properties[9] are shown in Table 2.

Operating conditions for five runs are given in Table 3.[23,24]

Verification of the proposed model has been carried out by comparing the computed results with experimental data from different feedstocks under a wide range of reaction

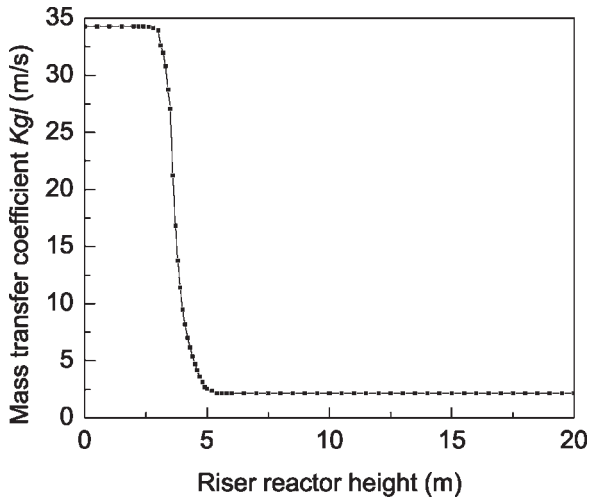

Figure 7. Axial distribution of mass transfer coefficient in dilute phase.

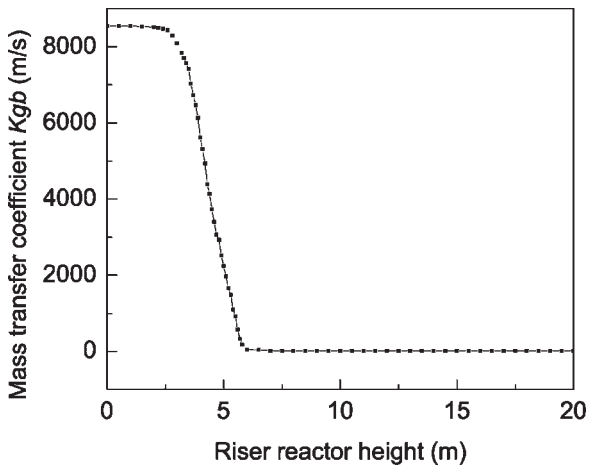

Figure 9. Axial distribution of mass transfer coefficient in the interphase between clusters and dilute phase.

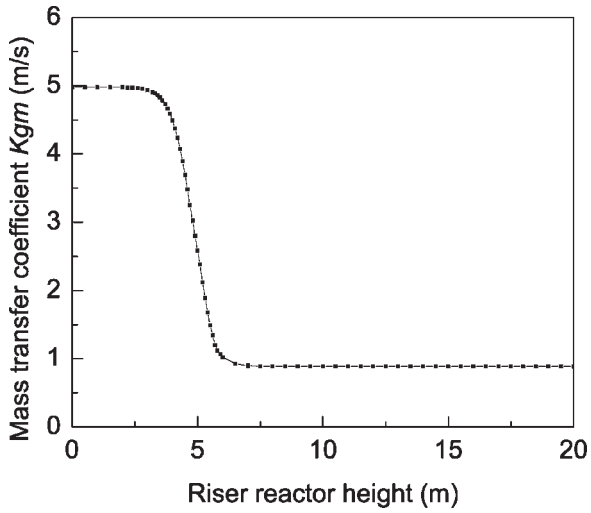

Figure 10. Axial distribution of mass transfer coefficient in the interphase between fluid in dilute phase and dynamic clusters.

conditions. These results are shown in Tables 4–8, respectively.

Table 4 shows the results for Run 1. The yield of gasoline calculated from the total yields of GP, GO, GN, and GA is 58.6%, with the relative error of 2.39%. The main conversions are cracking of paraffins and severe cracking of olefins, together with the production of aromatics, while naphthenes are much less converted. As the key lumps of the secondary reactions system, olefins (GO) are sharply reduced by 37.8% and LPG is significantly produced with the yield of 27.0%.

As shown in Table 5, gasoline yield in Run 2 is 75.0%, conversions are mainly taken place in the reactions related to olefins reduction and LPG production, while naphthenes are less converted, and the undesired products of DG and COKE are also less produced. Olefins are reduced by 25.5%, and the yield of LPG is 16.3%.

Table 6 shows the results of Run 3. In this case, gasoline yield is 65.8%, olefins are decreased by 26.5%, LPG yield is 23.1%, and aromatics are increased by 4.97%, while paraffins and naphthenes undergo slightly high conversion.

Results of Run 4 are shown in Table 7. The yield of gasoline is 68.1%, olefins are decreased by 31.4% due to the severe cracking of olefins, the cracking of paraffins and the production of aromatics are main conversion, while naphthenes are much less converted. The low temperature and high catalyst to oil ratio here lead to the low DG yield of 1.36% and the relatively high LPG yield of 21.0%.

Table 2. Properties of the Feedstocks

Feed Samples	1#Feed	2#Feed	3#Feed
Boiling range, K	305–451	310–459	312–439
Density at 293K, kg/m^3	708.4	732.4	705.8
Sulfur, μg/g	380	1427	288
Octane number, RON	90.6	91.3	90.5
Paraffins, vol %	34.3	30.7	36.1
Olefins, vol %	44.5	41.8	35.2
Naphthenes, vol %	7.4	9.4	13.7
Aromatics, vol %	13.8	18.1	15.0

Table 3. Operating Conditions for 5 Runs

Items	Run 1	Run 2	Run 3	Run 4	Run 5
Feedstocks	1#Feed	2#Feed	3#Feed	1#Feed	2#Feed
Reaction pressure, MPa	1.13	1.13	1.13	1.13	1.13
Reaction temperature, K	853	823	873	793	893
Vapor residence time, s	3.71	2.06	1.81	2.12	3.38
Catalyst to oil ratio	7.80	8.20	13.4	12.6	7.80

Table 8 gives the results for Run 5. Gasoline yield is 55.5%, olefins are greatly reduced by 36.7%, and LPG is significantly produced with the yield of 27.3%, while byproducts of DG and COKE are produced in 4.17% and 7.00%, respectively. The reason involved here is the high temperature and long residence time can promote the deep cracking of olefins and paraffins into low-molecular products.

From five sets of comparisons, it can be known that the computed results obtained from the multi-scale model agree well with the experimental data. The relative errors between experimental and calculated data are smaller than 7.5%, except for those of COKE. It is evidential that the proposed model is well constructed and is able to predict the P-O-N-A composition of gasoline from SRFCCG system under a wide range of operational conditions.

These results also suggest that the gasoline yield and the product distribution can be significantly affected by the properties of feedstocks and the reaction conditions such as reaction temperature, catalyst to oil ratio, vapor residence time. For example, higher temperature leads to the increase of LPG, DG, and the decrease in GO and gasoline yield. On the other hand, high gasoline yield and low olefins conversion are attributed to the relatively low temperature and short vapor residence time.

It should be noted that the olefins content in the upgrading gasoline can be reduced less than 18 vol % after secondary reactions, which enables the engine emission meet the EU IV emission standards and the new gasoline standard of DB11/238 in Beijing, China.

Prediction of product distribution

On the basis of the reliability of this model and the consistency of the simulation results with experimental data, another exercise has been preformed using another set of

Table 4. Comparison Between Computed Results and Experimental Data for Run 1

Items	Exp. Data		Comp. Results	Relative
	Inlet	Outlet	Outlet	Error
GO, wt %	44.5	6.69	7.18	7.32%
GP, wt %	34.3	23.6	24.0	1.67%
GN, wt %	7.40	6.52	6.66	2.14%
GA, wt %	13.8	21.8	22.2	1.83%
LPG, wt %	0	27.0	28.3	4.78%
DG, wt %	0	4.12	4.37	6.07%
LCO, wt %	0	5.13	4.96	−3.31%
COKE, wt %	0	4.93	2.75	−44.2%
Yield of Gasoline		58.6%	60.0%	2.39%

Table 5. Comparison Between Computed Results and Experimental Data for Run 2

Items	Exp. Data		Comp. Results	
	Inlet	Outlet	Outlet	Relative Error
GO, wt %	41.8	16.3	16.5	1.23%
GP, wt %	30.7	25.6	25.7	0.39%
GN, wt %	9.40	10.0	10.1	0.80%
GA, wt %	18.1	23.1	23.3	0.87%
LPG, wt %	0	16.3	16.8	2.94%
DG, wt %	0	1.61	1.68	4.35%
LCO, wt %	0	4.66	4.46	−4.29%
COKE, wt %	0	2.20	1.45	−34.1%
Yield of Gasoline		75.0%	75.6%	0.8%

Table 7. Comparison Between Computed Results and Experimental Data for Run 4

Items	Exp. Data		Comp. Results	
	Inlet	Outlet	Outlet	Relative Error
GO, wt %	44.5	13.1	13.3	1.83%
GP, wt %	34.3	27.2	27.7	1.92%
GN, wt %	7.40	7.89	8.09	2.53%
GA, wt %	13.8	19.9	20.2	5.09%
LPG, wt %	0	21.0	22.1	5.20%
DG, wt %	0	1.36	1.45	6.62%
LCO, wt %	0	5.17	5.03	−2.71%
COKE, wt %	0	3.92	2.10	−46.4%
Yield of Gasoline		68.1%	69.3%	1.76%

data (3#Feed, $P = 1.13$ MPa, $T = 823$ K, $t_v = 3.54$ s, Catalyst to oil ratio = 12.5) to simulate the lump concentration profile along with the riser height. Concentration variation of each lump for SRFCCG in riser reactor is plotted in Figure 11 where the experimental data is represented by the scattered points with the same symbols as the predicted results.

As shown, with the increase of riser reactor height, GP lump and GN lump first decrease rapidly and then keep decreasing slowly, whilst GO lump keeps reducing at a relatively high speed, while the LPG lump increases fast and finally reaches a larger concentration, when it comes to the other four lumps, they all keep increasing at a slow rate. Comparison of lump concentration at the riser reactor outlet shows predicted results agree with experimental data with acceptable accuracy, which indicates that simulation exercise is successful.

Because of the high activity of olefins, secondary reactions, such as alkylation, aromatization, etc., are easily taken place on GO to convert it into GA, LPG, and other lumps, leading to relatively fast decrease in GO and the increase of product lumps. Similarly, the decreases of GP and GN are attributed to their conversion into other lumps but with a relatively slow rate. Moreover, change in lumps concentration is proportional with their corresponding reaction rate. Since the stability of GA, secondary reactions are hardly taken place on it, which thus leads smooth change in the GA concentration. When it comes to the key production of LPG, the fast increase in LPG is due to the higher content of GA, GO, GN, and GP lumps are all easily converted into LPG. GA, GO, GN, GP, and LCO can be converted into DG and COKE, however, DG and COKE aren't consumed during the secondary reaction process. That is the reason why they keep increasing. The low increasing rate of DG and COKE is due to the control of reaction conditions.

Prediction of temperature distribution

Figure 12 gives the axial temperature profile of reactor along the riser height. As shown in this Figure, reactor temperature deceases sharply in the bottom region and slightly in the upper section. Sharp decreasing of temperature in the bottom zone is caused by large heat requirement of feedstock vaporizing at the riser inlet, and the endothermic secondary reactions on high-activity regenerated catalysts would further lower the reactor temperature. The predicted temperature at reactor outlet is consistent with the experimental one, which further demonstrates our simulation is successful. The trend of the predicted axial temperature profile is similar to the reported ones for commercial riser reactors.[11,25]

Conclusions

A new multi-scale model has been performed to simulate the heat transfer, mass transfer, momentum transfer, fluid flow with reactions together at different spatiotemporal scales of riser reactor for SRFCCG process. Multi-scale modeling method and multi-domain strategy have been successfully used to construct and integrate subscale models.

Table 6. Comparison Between Computed Results and Experimental Data for Run 3

Items	Exp. Data		Comp. Results	
	Inlet	Outlet	Outlet	Relative Error
GO, wt %	35.2	8.70	8.67	−0.35%
GP, wt %	36.1	26.0	25.9	−0.38%
GN, wt %	13.7	7.53	7.65	1.59%
GA, wt %	15.0	23.6	22.9	−2.97%
LPG, wt %	0	23.1	23.6	2.07%
DG, wt %	0	4.62	4.76	3.03%
LCO, wt %	0	4.52	4.34	−3.98%
COKE, wt %	0	3.25	2.13	−34.5%
Yield of Gasoline		65.8%	65.1%	−1.06%

Table 8. Comparison Between Computed Results and Experimental Data for Run 5

Items	Exp. Data		Comp. Results	
	Inlet	Outlet	Outlet	Relative Error
GO, wt %	41.8	5.06	5.14	1.58%
GP, wt %	30.7	19.9	20.2	1.51%
GN, wt %	9.40	6.28	6.39	1.75%
GA, wt %	18.1	24.3	24.8	2.06%
LPG, wt %	0	27.3	28.3	3.66%
DG, wt %	0	7.00	7.35	5.00%
LCO, wt %	0	5.15	5.04	−2.14%
COKE, wt %	0	4.17	2.81	−32.6%
Yield of Gasoline		55.5%	56.5%	1.80%

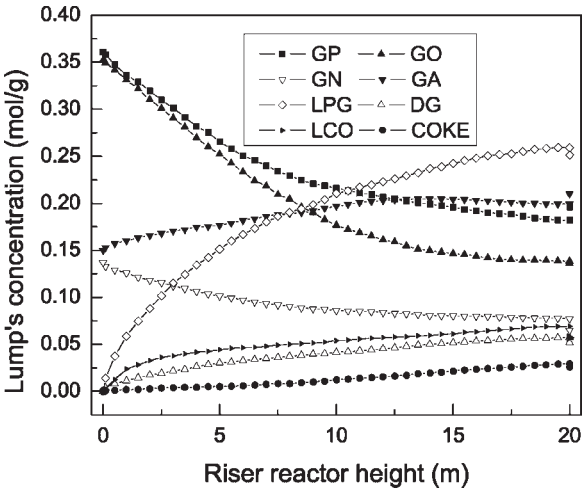

Figure 11. Lump concentration profile along with the riser reactor height.

Deeper insights of the mechanism details of SRFCCG have been obtained by simulation, such as the heterogeneous structures of fluid flow are caused by complex interaction between gas, particles, and clusters, which play a vital role in inhomogeneous level of the system; the transitional section is approximately from 4.5 to 6 m; and the mass transfer of the system has great effects on the secondary reactions, and it is dominated by mass transfer between clusters and dilute-phase.

Simulation results agree well with the experimental data for various cases. It is concluded that the current model is capable of predicting the heterogeneous structures of multiphase flow at the meso-scale, the reactor temperature profile and product distributions at the macro-scale of riser reactor for SRFCCG. It is also demonstrated that the multi-scale is well constructed and simulation exercise is successful, the multi-scale method can be served as a powerful modeling method for complex reaction system.

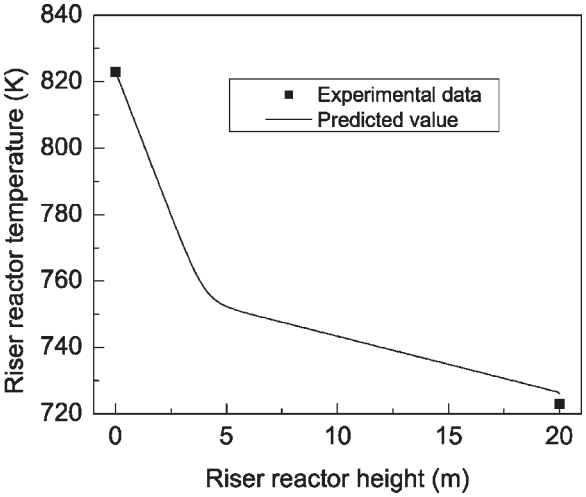

Figure 12. Axial temperature profile of the riser reactor.

Acknowledgements

Financial support for this work from the National Basic Research Program of China (973 Program, 2009CB219906), National Natural Science Foundation of China (20776117), and Specialized Research Fund for the Doctoral Program of Higher Education of China (20070698037) are gratefully acknowledged.

Notation

Ar = Archimedes number
b = volume fraction of cluster, dimensionless
Cp_g = specific heat capacity of the gas phase, kcal/kg·K
Cp_p = specific heat capacity of the particle phase, kcal/kg·K
d_p = particle diameter, m
D_{ab} = effective diffusion coefficient, m^2/s
D_d = cluster diameter, m
f = volume fraction of dense phase
g = gravity acceleration, m/s^2
G_v = gas flow rate, $g/cm^2 \cdot h$
$\triangle H$ = reaction enthalpy, kJ/kmol
k = volume faction of active component, dimensionless
K = inhomogeneous coefficient, dimensionless
K_j' = reaction rate constants of j lump, $m^3/g \cdot s$
l = equivalent diameter of cluster, m
m = mass of single particle, kg
m_p = total mass flow rate of particle phase, kg/s
m_g = total mass flow of gas phase, kg/s
N_{st} = energy consumption on suspending and transporting with respect to unit mass of particles, J/kg·s
r = radial distance, m
r_j = reaction rates of j lump, $mol/cm^3 \cdot h$
R = pipe radius, m
Re = Reynolds number, dimensionless
Sh = Sherwood number, dimensionless
Sc = Schmidt number, dimensionless
t = time, s
T = riser reactor temperature, K
U = superficial velocity, m/s
z = height coordinate with zero point at the bed bottom, m
z_0 = characteristic length for axial voidage profile, m

Greek letters

α = specific surface area of particles, m^2/m^3
α_j = concentration of j lump in gas, mol/g
α' = specific surface area of clusters, m^2/m^3
ε = voidage, dimensionless
ϕ = dimensionless radius
μ = viscosity, Pa·s
ρ = density, kg/m^3
v = kinematic viscosity, m^2/s

Subscripts

b = inter-phase between fluid in dilute phase and cluster
d = dense phase
f = fluid
g = gas
i = inter phase between dense and dilute phase
l = dilute phase
m = inter-phase between fluid in dilute phase and dynamic cluster
mf = minimum fluidization
o = center of the rising reactor
p = particle
s = slip velocity
w = wall

Literature Cited

1. John TM, Wojciechowski BW. On identifying the primary and secondary products of the catalytic cracking of neutral distillates. *J Catal*. 1975;37:240–250.

2. Li CY, Yang CH, Shan HH. Maximizing propylene yield by two-stage riser catalytic cracking of heavy oil. *Ind Eng Chem Res*. 2007;46:4914–4920.
3. Wang G, Xu CM, Gao JS. Study of cracking FCC naphtha in a secondary riser of the FCC unit for maximum propylene production. *Fuel Proc Technol*. 2008;89:864–873.
4. You HJ, Xu CM, Gao Js, Liu ZC, Yan PX. Nine lumped kinetic models of FCC gasoline under the aromatization reaction conditions. *Catal Commun*. 2006;7:554–558.
5. Mott RW, Roberie T, Zhao XJ, Davison G. *Suppressing FCC Gasoline Olefinicity While Managing Light Olefins Production*. NPRA Annual Meeting. San Francisco, 1998.
6. Ye XD, Jiao WZ, Liu YY. Chinese refinery uses new catalyst to meet olefin regulations. *Oil Gas J*. 2000;30:66–69.
7. Wang LY, Yang BL, Wang GL, Tang HT, Li ZB, Wei JL. New FCC process minimizes gasoline olefin, increase propylene. *Oil Gas J*. 2003;10:52–58.
8. Wang LY, Yang BL, Wang ZW, Yang XH. Secondary reactions of catalytically cracked gasoline. *J Chem Ind Eng*. 2005;56:841–846.
9. Yang BL, Zhou XW, Chen C, Yuan J, Wang LY. Molecule simulation for the secondary reactions of fluid catalytic cracking gasoline by the method of structure oriented lumping combined with Monte Carlo. *Ind Eng Chem Res*. 2008;47:4648–4657.
10. Wang LY, Yang BL, Wang ZW. Lumps and kinetics for the secondary reactions in catalytically cracked gasoline. *Chem Eng J*. 2005; 109:1–9.
11. Gao JS, Xu CM, Lin SX, Yang GH, Guo YC. Advanced model for turbulent gas–solid flow and reaction in fcc riser reactors. *AIChE J*. 1999;45:1095–1113.
12. Theologos KN, Markatos NC. Advanced modeling of fluid catalytic cracking riser-type reactors. *AIChE J*. 2004;39:1007–1017.
13. Li JH, Cheng CL, Zhang ZD, Yuan J, Nemet A, Fett FN. The EMMS model-its application, development and updated concepts. *Chem Eng Sci*. 1999;54:5409–5425.
14. Li JH, Zhang JY, Ge W, Liu XH. Multi-scale methodology for complex systems. *Chem Eng Sci*. 2004;59:1687–1700.
15. Li JH, Kwauk M. *Particle–Fluid Two-Phase Flow—The Energy-Minimization Multi-Scale Method*. Beijing: Metallurgical Industry Press, 1994.
16. Ingram GD, Cameron IT, Hangos KM. Classification and analysis of integrating frameworks in multiscale modelling. *Chem Eng Sci*. 2004;59:2171–2187.
17. Li JH, Kwauk M. *The dynamics of fast fluidization*. In: Grace JR, Master JM, editors. *Fluidization*. New York: Plenum Press, 1980:537–544.
18. Cheng CL, Li JH, Zhang ZD, Yuan J. Fluid dynamic model of concurrent-up gas–solid two-phase flow. *J Chem Ind Eng*. 2001; 52:684–689.
19. Halder PK, Basu P. Mass transfer from a coarse particle to a fast bed of fine solids. *AICHE Symp Ser*. 1988;84:58–64.
20. Moustafa TM, Froment GF. Kinetic modeling of coke formation and deactivation in the catalytic cracking of vacuum gas oil. *Ind Eng Chem Res*. 2003;42:14–25.
21. Aiouache F, Goto S. Reactive distillation-pervaporation hybrid column for tert-amyl alcohol etherification with ethanol. *Chem Eng Sci*. 2003;58:2465–2477.
22. Xu BL, Fan YN, Zhang Y, Tsubaki N. Pore diffusion simulation model of bimodal catalyst for Fischer-Tropsch synthesis. *AIChE J*. 2005;51:2068–2076.
23. Wang ZW, Yang BL, Chen C, Yuan J, Wang LY. Modeling and optimization for the secondary reaction of FCC gasoline based on the fuzzy neural network and genetic algorithm. *Chem Eng Proc*. 2007;46:175–180.
24. Chen C, Yang BL, Yuan J, Wang ZW, Wang LY. Establishment and solution of eight-lump kinetic model for FCC gasoline secondary reaction using particle swarm optimization. *Fuel*. 2007;86: 2325–2332.
25. Berry TA, McKeen TR, Pugsley TS, Dalai AK. Two-dimensional reaction engineering model of the riser section of a fluid catalytic cracking unit. *Ind Eng Chem Res*. 2004;43:5571–5581.

Manuscript received Jun. 11, 2008, and revision received Nov. 28, 2008.